RESEARCH ARTICLE

Rheological study on 3D printability of alginate hydrogel and effect of graphene oxide

Huijun Li[1,2], Sijun Liu[2] and Lin Li[1,2,*]

[1] Singapore Centre for 3D Printing (SC3DP), School of Mechanical and Aerospace Engineering, Nanyang Technological University (NTU), 50 Nanyang Avenue, Singapore 639798, Singapore

[2] School of Mechanical and Aerospace Engineering, Nanyang Technological University, 50 Nanyang Avenue, Singapore 639798, Singapore

Abstract: In recent years, hydrogels have been used as important biomaterials for 3D printing of three dimensional tissues or organs. The key issue for printing a successful scaffold is the selection of a material with a good printability. Rheological properties of hydrogels are believed to pay an important role in 3D printability. However the relations between rheological properties of hydrogels and 3D printability have not been extensively studied. In this study, alginate-based hydrogels were prepared as a model material for an extrusion-based printer and graphene oxide was added to modify the rheological properties and 3D printability of the hydrogels. Rheological studies were performed for the hydrogel samples with different formulas. The range of shear rates that the hydrogels suffered during the printing process was deduced. This range of shear rates helped us to select a proper shear rate to investigate the thixotropic properties of the hydrogels. Furthermore, we also defined some measureable parameters to describe and discuss the quality of 3D printing. The present study shows a new approach to analysis of 3D printability of a hydrogel and also provides some suggestion for 3D printing of 3D scaffolds.

Keywords: printability, rheology, 3D printing, alginate hydrogel, graphene oxide

*Correspondence to: Lin Li, School of Mechanical and Aerospace Engineering, Nanyang Technological University, 50 Nanyang Avenue, Singapore 639798, Singapore; Email: mlli@ntu.edu.sg

Received: April 5, 2016; **Accepted:** June 14, 2016; **Published Online:** June 24, 2016

Citation: Li H, Liu S and Li L, 2016, Rheological study on 3D printability of alginate hydrogel and effect of graphene oxide. *International Journal of Bioprinting*, vol.2(2): 54–66. http://dx.doi.org/10.18063/IJB.2016.02.007.

1. Introduction

Due to the limitations of organ transplantation such as the shortage of donors, tissue engineering was introduced in the early 1970s. Tissue engineering aims to fabricate artificial organs or tissues to replace damaged or diseased ones in the human body. The artificial substitute tissues and organs can be customized, which means that a patient's own cells can be used to regenerate substitute organs and tissues. It has an obvious advantage that immunization response and rejection can be overcome. However, without a three dimensional complex geometry, the artificial tissues or organs cannot transport nutrients, exchange oxygen and remove waste. Due to the high potential and development of 3D printing technologies[1–3], fabrication of complex tissues or organs may come true.

Hydrogels have attracted a great attention as biomaterials for 3D printing due to their soft and wet nature as well as similarities to biological tissues. There is a great success for application of hydrogels in the area of 3D printing[4–12] for regeneration and repair of tissues or organs[4,10–12]. Alginate as one of biomaterials is widely used in various pharmaceutical and medical applications but displays some unsatisfactory

properties such as poor mechanical strength and lack of structural integrity, which limits its applications. Recently, much effort has been made for improving the performance of alginate based scaffolds. Compounding of alginate with other polymers such as pectin[13] or chitosan[14] has been found to provide just a marginal effect. Meanwhile, graphene oxide (GO) has attracted a great attention in various fields including tissue engineering because of its novel properties such as good electric conductivity, thermal conductivity, mechanical stiffness, and biocompatible properties[15–18]. GO sheets have been reported to be ultra-strong and biocompatible; therefore, GO is a desirable nanomaterial for modifying scaffolds used in tissue engineering[19]. The functional groups on GO sheets may improve interfacial interaction between GO and a polymer matrix, which paves the pathways for developing GO based nanocomposites with remarkable mechanical properties[20]. For example, Fan *et al*. reported a significant increase of elastic modulus of chitosan by about 200% with the addition of small amount of graphene oxide[17]. Mariana *et al*. reported that GO/alginate films showed superior thermal and mechanical properties compared with alginate[21]. However, the effect of GO on the alginate hydrogel has not been extensively studied in the literature.

In recent years, many researchers and scientists have investigated the printability of materials for extrusion-based printing. The word, printability, not only means how easy a hydrogel can be printed out by a 3D printer, but also implies how stable a printed 3D construct or scaffold is. The latter is more important in real applications of bio-fabrication. For example, Chung's group found that the alginate-gelatin hydrogel had to be printed at low temperatures as the gelation temperature for alginate-gelatin hydrogels is around 11°C[22]. Jia *et al*. evaluated the printability of hydrogel by using a point-to-point strategy to print several dots and found that the plot of dots areas and viscosity can directly shows the relationship between printability and viscosity of different samples. Meanwhile, the results indicated that the optimal range of kinematic viscosity for a piston driven system is from about 400 to 3000 mm^2/s[6]. Murphy *et al*. concluded that there are many factors influencing the printability of materials, such as pressure, flow rate, viscosity, etc. They summarized a range of viscosities for different 3D bio-printers (inkjet, extrusion-based and laser assisted) based on the previous studies and concluded that the sample with the range of viscosity (30 mPa.s to $> 6 \times 10^7$ mPa.s) is suitable for an extrusion-based printer[3]. Thus, rheological properties of potential hydrogels for an extrusion based printer are considered to be a key factor in controlling the printability of the hydrogels and the fidelity of the printed 3D structures. However, the relationship between rheological properties of hydrogels and 3D printability has not been systematically studied in the literature.

A printable hydrogel needs to be optimized to have low viscosity during printing and sufficient mechanical strength after printed. So, it is ideal for a printable hydrogel to have a thixotropic property and fast recovery ability. However, most of the materials could not recover their properties immediately and the recovery time depends on the materials and shear rate. To improve the quality of printing, it is important to choose a material with excellent thixotropic properties and print the material with a reasonable recovery time. For a non-Newtonian fluid, viscosity is a function of shear rate in a printing syringe. Finding the relationship between piston speed and shear rate for an extrusion based printing process is fundamentally important. Furthermore, to study the thixotropic property one should know the shear rate that is generated by the piston speed. It is also important to know whether the breakdown of crosslinks by shearing is reversible after removing the shear force.

In this study, alginate-based hydrogels were chosen as a basic printing material for an extrusion-based printer. Rheological studies were performed for the samples with different formulas. The range of shear rate that the hydrogels suffered during printing was deduced. This range of shear rates helped us to select a proper shear rate to investigate the thixotropic properties of the hydrogels. Graphene oxide (GO) was added to modify the rheological properties and 3D printability of the hydrogels. Furthermore, some measureable parameters were defined for quantifying the quality of 3D printing.

2. Materials and Methods

2.1 Materials and Sample Preparation

Sodium alginate was purchased from Sigma-Aldrich, Singapore. According to the supplier, the molecular weight of the sodium alginate ranged from 100,000 to 150,000 g/mol and the G block content was 50%–60%. Calcium chloride with 99% ACS grade was obtained from Sigma-Aldrich, Singapore. Graphene oxide (GO) was a product of XF NANO (Nanjing, China). All

materials were used without further purification.

Aqueous solutions of alginate with various concentrations (2, 4, 6, 8 and 10 wt.%) were prepared using deionized water from a Millipore water purifier. Then, calcium chloride solutions with various molar fractions were added to each solution of alginate to obtain alginate hydrogels with various $CaCl_2$ contents. In order to study the effect of GO on alginate hydrogels, alginate composite hydrogels filled with various GO contents were prepared as follows. First, the suspensions with various GO contents were produced by ultrasonic treatment using deionized water. After that, 5 g of alginate powder (for a final concentration of 10 wt.% based on the total weight of DI water) was added into the suspension of GO under magnetic stirring. Finally, alginate composite hydrogels were prepared by adding a certain amount of calcium chloride solution into the solution of GO/alginate under magnetic stirring. The alginate concentration in the composite hydrogels was fixed 10 wt.% and a $CaCl_2$ content of 25 mM/L was also kept constant, while GO was loaded to 0.05, 0.15 and 0.25 wt.% based on total deionized (DI) water. The prepared samples were labeled with GO_a/Alg_b, where *a* and *b* are the weight fraction of GO and alginate, respectively.

2.2 Shear Rate in an Extrusion-based 3D Printing Process

During an extrusion-based 3D printing process, molecular crosslinks of hydrogels may have broken down by shear forces, reducing viscosity, and allowing highly viscous hydrogels to be extruded out from the printing nozzle. A printable hydrogel needs to be optimized to have low viscosity during printing but sufficient mechanical strength after printed. So, it is ideal for a printed hydrogel to have a thixotropic property and then a recovery ability, which means that viscosity of the hydrogel is low when a shear force is applied but the viscosity recovers quickly after the shear force is removed. A material is said to be thixotropic when its apparent viscosity decreases with time under a constant shear rate. As for thixotropic materials, the best-known example is the thixotropic paints and the other examples include concentrated suspensions, drilling fluids, emulsions, protein solutions, laponite, and silk nanofibril-based hydrogel[23–26].

The 3D printing head consists of a piston, a syringe, and a nozzle. The syringe and nozzle possess different inner diameter. Before printing, the hydrogels are loaded into the syringe firstly, and then it is extruded to the nozzle under the pushing action of a piston. Based on the fluid mechanics[27], the viscosity is a function of shear rate. At a constant volume flow rate, the linear flow rate in a pipe will change when the cross section area of the pipe is changed. Therefore, the linear flow rate will change due to the change in the cross section area from the syringe to the nozzle, which also results in a change in the shear rate. Shear rate is an important factor for an extrusion based printer. In this study, the range of shear rates in the syringe is estimated from a given piston moving speed of the 3D printer.

Consider a laminar and steady flow of a time-independent and incompressible fluid in a circular pipe of radius, R, as shown in Schematic 1A. Since there is no angular velocity, the force balance in the *z* direction on a fluid element situated at a radius *r* ($0 < r < R$) can be written as

$$p(\pi r^2) - (p + \Delta p)\pi r^2 = 2\tau\pi rL \tag{1}$$

$$\tau = \frac{-\Delta P}{2L} r \tag{2}$$

where p is the pressure, τ is the shear stress on the surface of the cylindrical element and L is the length of the element. **Equation (2)** shows the shear stress distribution across the cross-section of pipe, whereas the shear stress being zero at the axis of the pipe (Schematic 1B). Note that **Equation (2)** is applicable to both turbulent and laminar flows of any fluid since it is based on a simple force balance and also no assumption has been made[27].

For a power-law fluid in a pipe, shear stress is a function of shear rate as follows[28]:

$$\tau = m(\dot{\gamma})^n \tag{3}$$

where n and m are the power-law index and power-law consistency coefficient, respectively, whereas $\dot{\gamma}$ is the shear rate. The viscosity for the power-law fluid can be described by

$$\eta = m\left(\dot{\gamma}\right)^{n-1} \tag{4}$$

So, the shear rate can be written as

$$\dot{\gamma} = \frac{du}{dr} = \frac{-\Delta P}{2\eta L} r \tag{5}$$

where u is the flow velocity at r. Integrating the equation, we can get the velocity in the pipe

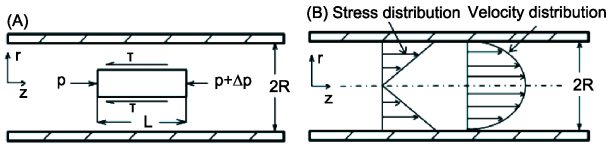

Schematic 1. (A) Flow through a pipe, and **(B)** Stress and velocity distribution of non-Newtonian flow in a pipe.

$$u = \frac{-\Delta P}{4\eta L}(R^2 - r^2) \quad (6)$$

Rheological study was conducted on the alginate based hydrogels with different concentrations using a plate rheometer. Based on the power-law model and experimental data, the constant m and n for each sample can be obtained through curve fitting. These two parameters will be used in further calculation to deduce the shear rate that the hydrogel undergoes during the printing process.

Assuming that in the syringe there is a uniform flow rate (V), the volumetric flow rate (Q) of a non-Newtonian fluid can be written as follows[27]

$$Q = \pi R^2 V = \pi \left(\frac{n}{3n+1}\right)\left(\frac{-\Delta p}{2mL}\right)^{\frac{1}{n}} R^{\left(\frac{3n+1}{n}\right)} \quad (7)$$

where L and Δp are length of the syringe and the pressure drop, respectively.

Then the pressure drop can be expressed as follows

$$\Delta p = -2mL\left[\frac{VR^2}{\left(\frac{n}{3n+1}\right)\left(R^{\frac{3n+1}{n}}\right)}\right]^n \quad (8)$$

The shear rate $\dot{\gamma}$ in the pipe can be described as follows

$$\dot{\gamma}^n = \left[\frac{VR^2}{\left(\frac{n}{3n+1}\right)(R^{\frac{3n+1}{n}})}\right]^n .r \quad (9)$$

Assuming that the volume of hydrogels does not change before and after printing,

$$V_2 = V_1\left(\frac{D_1}{D_2}\right)^2 \quad (10)$$

where D_1 is the inner diameter of the syringe, V_1 is the speed of the piston, D_2 is the inner diameter of the nozzle, and V_2 is the speed of extruded hydrogel in the nozzle,

From **equation (9)**, the shear rate $\dot{\gamma}$ in the syringe can be calculated from the following equation

$$\dot{\gamma}_1^n = \left[\frac{V_1 R_1^2}{\left(\frac{n}{3n+1}\right)(R_1^{\frac{3n+1}{n}})}\right]^n .r \quad (11)$$

The shear rate $\dot{\gamma}$ in the nozzle can be calculated from the following equation

$$\dot{\gamma}_2^n = \left[\frac{V_2 R_2^2}{\left(\frac{n}{3n+1}\right)(R_2^{\frac{3n+1}{n}})}\right]^n .r \quad (12)$$

2.3 Rheological Evaluations of Alginate Hydrogels

The rheological properties of the alginate hydrogels were measured by using a rotational rheometer (DHR, TA Instruments, USA). A 40 mm parallel plate with a measurement gap of 0.55 mm was used. First of all, strain sweeps in the range of 0.1%–100% at the frequencies of 0.1–2.0 Hz were carried out in order to determine the linear viscoelastic range of the samples. The following three rheological experiments at room temperature were adopted in order to explore the rheological properties of samples: (1) frequency sweep tests over an angular frequency range of 0.01–100 rad/s at a constant strain of 2%; (2) steady-state flow tests in a range of shear rate 0.5–500 s^{-1}; and (3) recovery tests under a low shear rate.

2.4 Fabrication of 3D Structure

An extrusion-based printer for scaffold fabrication was employed in this study. The printing system consists of two parts: a high precision displacement pump (TechnoDigm, PDP 1000, Singapore) and a desktop xyz motor (TechnoDigm, DR3331T-EX, Singapore). The printing head was mounted on the printing system to print along the preprogrammed tracks with an adjustable speed (15 mm/s used in this study). The printing head consists of a piston, a syringe, and a changeable nozzle. The displacement pump drives the piston with a controllable speed (0.009 mm/s) to extrude hydrogels from the syringe on a glass slide. The 3D scaffolds were fabricated at room temperature. Firstly, a 3D structure to be printed was preprogrammed on the 3D printing system to define the extrusion route for the hydrogel. Secondly, the hydrogel was loaded into the syringe and then the syringe was installed on the dispensing unit. Under the action of the piston at the speed as mentioned previously, the hydrogel loaded in the syringe was extruded through a 0.25 mm nozzle while the dispenser was moving at a defined speed. Once the first layer was formed, the nozzle was lift up and then continued to move along the preprogrammed tracks at the same speed to form the second

layer. Subsequent layers were added layer-by-layer in the vertical axis.

3. Results and Discussion

3.1 Sol-gel Transition

Alginate is able to form a gel in the presence of $CaCl_2$. Figure 1 illustrates the dependence of storage modulus G' and loss modules G" on angular frequency ω for the aqueous solution of 2 wt.% alginate containing various $CaCl_2$ contents. At low $CaCl_2$ contents, such as 2.5, 3.75 and 5 mM/L, G" is larger than G' in the low frequency region. These correspond to the viscoelastic properties of a polymer fluid without entanglements. After adding 6.25 mM/L of $CaCl_2$ into the alginate solution, both the G' and G" become much higher than those at 5 mM/L of $CaCl_2$ in the whole frequency region. It is noted that G' is larger than G", showing a characteristic of a solid-like material. There is an obvious gap between the curves for 5 mM/L and 6.25 mM/L. The large increase from the G' curve at 5 mM/L of $CaCl_2$ to that 6.25 mM/L of $CaCl_2$ implies that the gelation of alginate solution takes place at a $CaCl_2$ ions concentration between 5 mM/L and 6.25 mM/L. The frequency dependences of G' and G" for the solutions of other alginate concentrations are similar to that observed in Figure 1 (data not shown). The only difference is that the $CaCl_2$ content corresponding to the region of the gelation increases with increasing alginate concentration.

Based on Figure 1, it can be found that the sol-gel transition takes place between 5 mM/L and 6.25 mM/L of $CaCl_2$ for 2 wt.% alginate solution. In order to determine the exact critical gel concentration, we followed a method developed by Winter and Chambon[29]. The main feature of this method is the scaling law at the gel point: both G'(ω) and G"(ω) are proportional to ωn ($0 < n < 1$) at sufficiently low frequencies, ω. The definition of the gel point by this power-law is excellent because the gelation variable will lose its dependency of frequency at the gel point. Several works have shown that this method is reliable and valid for determination of the gel point for various polymer gels with different gelation mechanisms[30–33]. Figure 2(a) shows the application of the Winter-Chambon method to the solution of 2 wt.% alginate within the sol-gel transition region. The gel point is determined through the multi-frequency plots of loss tangent versus $CaCl_2$ content. All curves pass through the common point at a certain $CaCl_2$ content of 5.73 mM/L, and this point is defined as the critical gel concentration (Cg) for the solution of 2 wt.% alginate. The similar multi-frequency curves of loss tangent versus $CaCl_2$ content have also been observed for other alginate solutions, and the critical gel concentrations obtained are shown in Figure 2(b). It is observed that Cg increases linearly with increasing alginate concentration, indicating that much more $CaCl_2$ are required to cross-link alginate chains into infinite gel networks at a higher alginate concentration.

3.2 Rheological Evaluation

One of the aims in this study is to determine whether 3D extrusion printing could be used to print hydrogels formed through ionic association. In order to understand the printability of alginate hydrogels, it is important to know its rheological properties. Figure 3(a) shows the flow curves over a range of shear rates (0.5−500 s^{-1}) for alginate hydrogels at a fixed $CaCl_2$ content of 25 mM/L. A shear-thinning behavior was observed for all samples and the effect of alginate

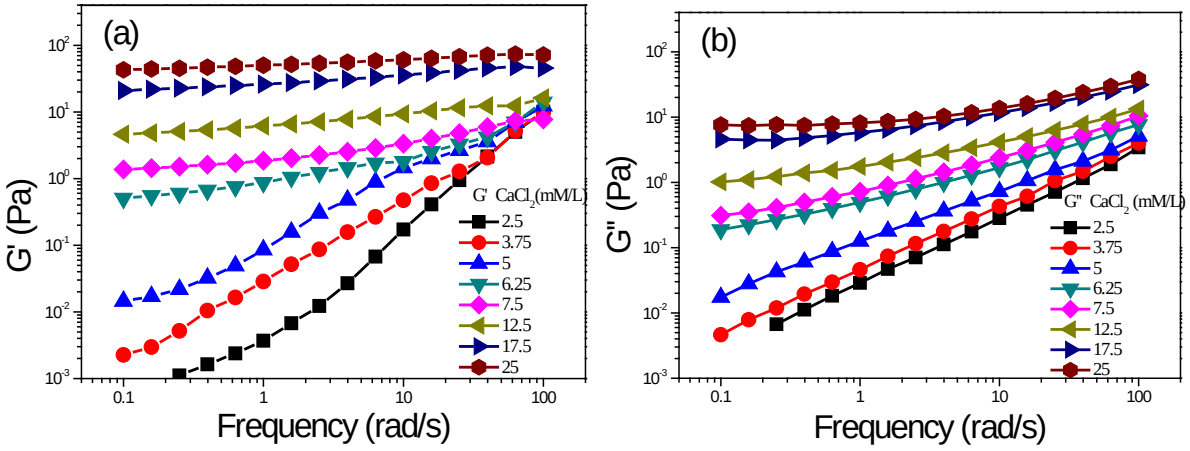

Figure 1. Dependence of G' and G" on angular frequency for 2 wt.% alginate solution with various contents of $CaCl_2$.

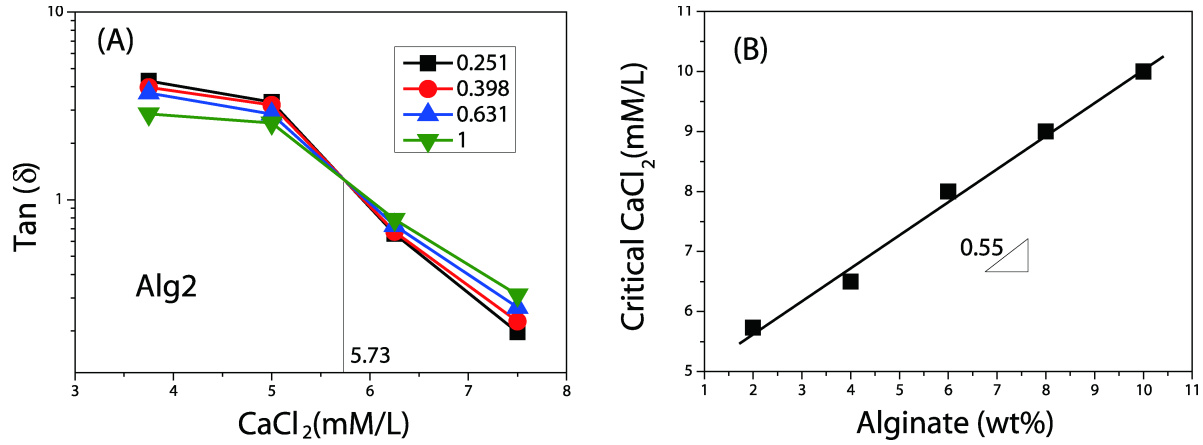

Figure 2. (a) Dependence of tan δ on $CaCl_2$ content for 2 wt.% alginate solution at different angular frequencies in rad/s as indicated in the inset, and **(b)** relationship of the Cg with alginate concentration.

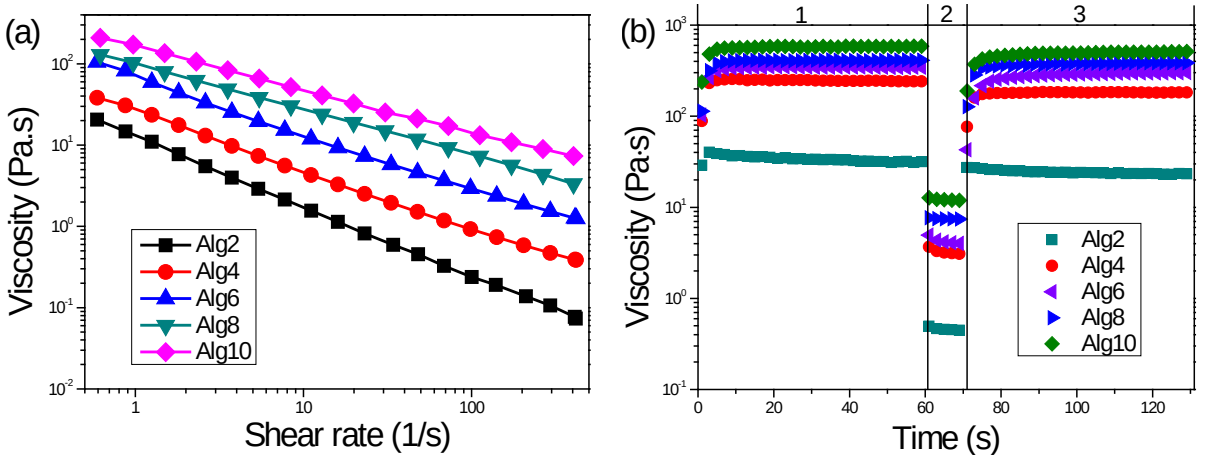

Figure 3. (a) Viscosity as a function of shear rate at room temperature, and **(b)** effect of various alginate concentrations on the recovery behavior of alginate hydrogels at a fixed $CaCl_2$ content of 25 mM/L.

concentration on viscosity is significant. The viscosity increases with increasing alginate concentration and decreases with shear rate. This is the most common behavior of a non-Newtonian fluid[27]. Specially, the influence of shear rate on viscosity for the 2 wt.% alginate solution is more significant than that for the 10 wt.% alginate solution. This viscosity will affect the amount of hydrogel extruded from the printing nozzle and the printing quality.

An ideal printable hydrogel should be highly thixotropic, which means that viscosity of the hydrogel become low quickly when applying a shear force but the viscosity recovers quickly after the shear force is removed. It is also important to know how the crosslinks of the hydrogel can recover before the next layer starts to be printed. Thixotropic properties and recovery times were investigated by applying a steady shear rate. Thus, before conducting the rheological test, we should know the appropriate value of shear rate. As discussed in the Section 2.2, the shear rate can be calculated using **Equation (12)**. Firstly, rheological measurements were performed on hydrogel samples using a rheometer. Based on the power-law model as described in **Equation (4)** and experimental data, the constants m and n for each sample can be obtained through curve fitting. The details of the samples and the values of m and n are given in Table 1. The viscosity of 2 wt.% alginate hydrogel is too low, so that the printed scaffold could collapse quickly. Thus, this sample is not appropriate for 3D printing. For the other concentrations of hydrogels (see Table 1), the maximum shear rate in the nozzle for each sample is around 100 s^{-1} at the printing speed of 0.009 mm/s used in this study, where the diameter of the syringe and the nozzle are 3.88 mm and 0.25 mm, respectively. Thus, we will examine the thixotropic properties of each

Table 1. Changes of m and n obtained through curve fitting as well as the maximum shear rate in the nozzle for each sample with alginate concentration at a fixed $CaCl_2$ content of 25 mM/L

Samples	m	n	Shear rate (s^{-1})
Alg2	12.5	0.147	170.5
Alg4	25.4	0.288	112.8
Alg6	64.8	0.329	105.2
Alg8	115.3	0.390	97.0
Alg10	172.5	0.424	93.4
GO0.05/Alg10	223.9	0.399	96.0
GO0.15/Alg10	257.4	0.355	101.4
GO0.25/Alg10	360.2	0.305	109.5

sample under a shear rate of 100 s^{-1}.

The whole test consisted of three steps. At Step I, a shear rate of 0.1 s^{-1} was applied for 60 seconds. This step simulated the initial state of a hydrogel before printing. At Step II, the shear rate was increased to 100 s^{-1} and held for 10 seconds. This step simulated the condition for a hydrogel under a certain shear rate during the printing process. At Step III, the shear rate was reduced to 0.1 s^{-1} and held for 60 seconds to simulate a condition similar to the final state of the hydrogel after printing. Figure 3(b) shows the recovery behavior of the viscosity of $CaCl_2$/alginate hydrogels. In the case of the Alg10 hydrogel at step I, the initial viscosity was 582 Pa.s. Then, the viscosity sharply decreased to 11.87 Pa.s when the shear rate was increased to 100 s^{-1}. After removing the shear rate, the viscosity built up to 465 Pa.s in about 10 seconds, which was a 79.7% recovery of the initial value. If the hydrogel was given a much longer recovering time (20 seconds), the viscosity could recover to 484 Pa.s (83% of the initial value). The hydrogel could recover its viscosity by 85.5% of the initial value after 30 seconds, but the viscosity could not recover further even with longer recovery time. The reason for the viscosity of a hydrogel to recover after a period of rest is because the broken crosslinks caused by shearing need some times to rebuild. The recovery time decreases as the alginate concentration increases, but most of the samples tested in this study could not recover in few seconds and they need more than 30 seconds to recover their viscosities to 83% of the initial values.

From Table 1, several features can also be observed. As the concentration of alginate increased from 2 wt.% to 10 wt.%, its power-law consistency coefficient (*m*) and power-law index (*n*) increased. This is explained through an increased number of polymer chains at a higher mass concentration. Thus, the viscosity increases as the polymer concentration increases[34]. Similarly, *m* and *n* gradually increased as the viscosity increases. For a shear-thinning fluid, *n* should be smaller than 1[27]. All the tested samples showed that the values of n are smaller than 1, indicating that all samples have the shear-thinning properties, as proved in Figure 3(a). Furthermore, as the concentration of alginate increased from 2 wt.% to 10 wt.%, the extent of shear-thinning became gentler. This implies that an alginate hydrogel with a higher concentration shows a weaker shear-thinning behavior than the one with a lower alginate concentration; whilst the former has a bigger value of *n*. This phenomenon was also mentioned and discussed in Chhabra and Richardson's book[27]. If the value of *n* can achieve one, the viscosity will be a constant and not dependent on shear rate. For the case of shear-thinning fluid ($0 < n < 1$), the fluid behaves more like a Newtonian fluid when the value of *n* approaches to 1.

3.3 Fabrication of 3D Structures

Printing a hydrogel into a 3D scaffold in the vertical direction is very challenging. The strength of the hydrogel material must be strong enough to withstand the weight of the entire structure. This is quite difficult for hydrogels as they are soft materials with high water content. Insufficient structural strength of the hydrogel base can result in the collapse of the scaffold in the vertical configuration. Thus, the viscosity and mechanical strength of the hydrogel material has to be relatively high in order to suffer the compressive pressure resulted from the upper layers of the scaffold structure.

In this study, the controllable push speed of the piston is 0.009 mm/s, the inner diameter of the microneedle is 250 μm, and the volume of the syringe is 5 cm^3. In order to study the stability and quality of printing, we took the images of the printed constructs. Figure 4 shows the effect of various alginate concentrations on the structure of printed hydrogel scaffolds at a fixed $CaCl_2$ content of 25 mM/L. The printed scaffold shown in Figure 4 comprised of 9 layers and these pictures were taken at the initial time. It is apparent that for the scaffold printed with a higher alginate concentration, the printed filaments were of more uniform width and the shape was more stable. If the filament width was defined as d, it can be found from Figure 4(f) that d decreases with increasing alginate concentration. This is because that the hydrogel with a higher concentration of alginate was stronger and not

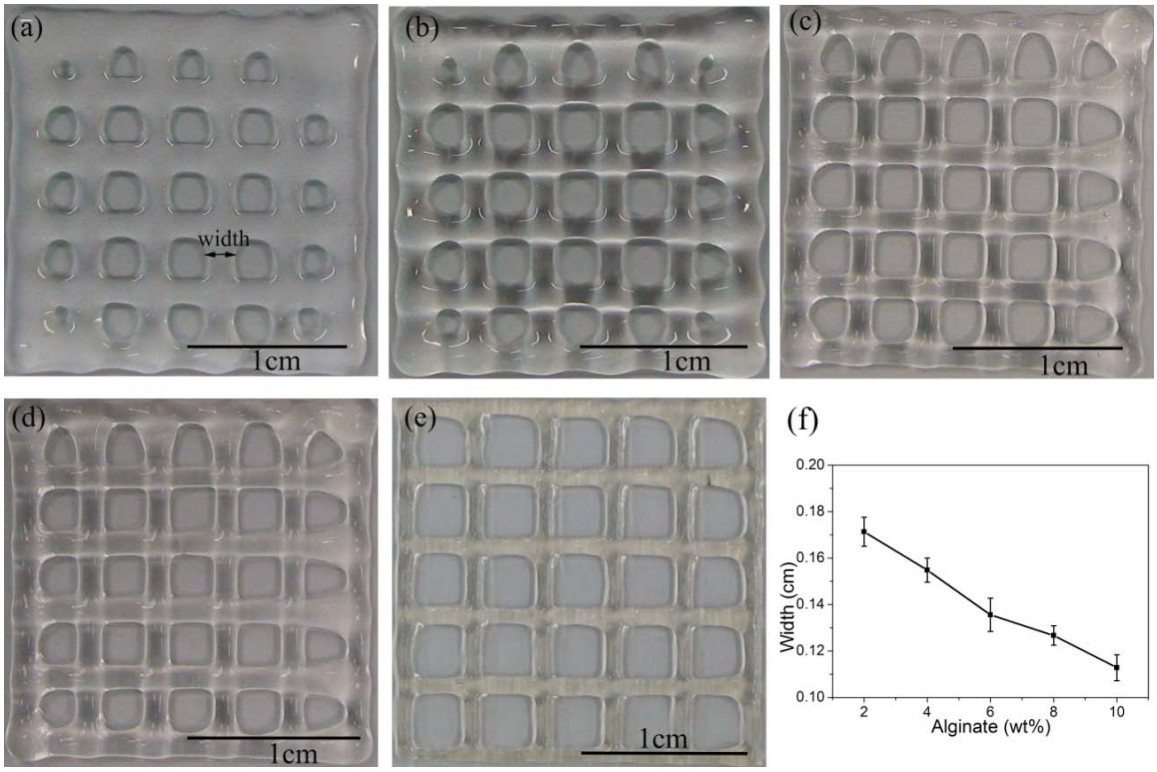

Figure 4. The images of printed hydrogel scaffolds with various alginate concentrations. **(a)** 2 wt.%; **(b)** 4 wt.%; **(c)** 6 wt.%; **(d)** 8 wt.%; **(e)** 10 wt.% alginate hydrogels at a fixed $CaCl_2$ content of 25 mM/L; **(f)** the effect of various alginate concentrations on filament width.

easy to collapse compared to the hydrogel with a low alginate concentration. Thus, a smaller width implies a better printing quality of the scaffold.

We also observed the time dependence of the printed structures from time 0 to 20 minutes. Figure 5 shows the images of printed hydrogel scaffolds at different ageing times and the relationship between width and ageing time for 2 wt.% alginate hydrogels added with a fixed $CaCl_2$ content of 25 mM/L. It is obvious that the shape of the scaffolds changed with time as the hydrogel was soft and easy to collapse. On the other hand, the filament width broadens with ageing time. The effect of ageing time on the filament width for other alginate hydrogels are similar to those observed in Figure 5 (data not shown).

3.4 Effect of GO on 3D Printability of Alginate Hydrogels

Alginate composite hydrogels filled with various GO contents were used as a printing material in this section to study on how GO could improve the 3D printability of alginate hydrogels. The printed scaffold discussed in this section has 50 layers. From Figure 6(a), it is observed that the hydrogels filled with GO also show the shear-thinning properties. GO can increase the viscosity of hydrogels, whilst viscosity increases with increasing content of GO. On the other hand, it is shown that the hydrogels with various GO contents also reveal the thixotropic properties (Figure 6(b)).

Figure 7(a) shows the effect of GO on the morphologies of the printed scaffolds with 10 wt.% alginate hydrogels. The higher concentration of GO produced a structure with a thinner width. GO is essentially an atomic sheet with a large number of functional groups (e.g., hydroxyl, epoxide, and carbonyl groups) bound on the surface. After adding GO into the alginate solution, the functional groups from GO such as (-OH, and -COOH) will interact with the groups (-OH) from calcium alginate. Thus, a large amount of hydrogen bonds formed between the GO and alginate may significantly improve the rheological properties of the composite hydrogels.

Furthermore, the traditional process of 3D printing is to print a scaffold layer-by-layer and there is no pause between the two layers. However, printing of a scaffold continuously on one layer after another without any pause seems unreasonable for an extrusion based printer, because the viscosity of the extruded

material maybe quickly decrease when being printed and it needs a period of time to recover its viscosity. We here define the recovery time as the duration from the finishing time of a current layer printed until the printer starts to print and deposit a new layer on the current layer. Therefore, it would be necessary to find a reasonable recovery time that can improve the quality of printing. Based on the previous discussion in Section 3.2, a recovery time of 30 seconds was set as the extruded hydrogels would recover most of its viscosity after 30 seconds, and the viscosity could not recover more significantly with longer recovery time. After that, we found that the quality of printing was obviously improved, as proved by comparing the images of the printed scaffolds shown in Figure 7(b).

Figures 7(c) and (d) show the effect of GO content on the width and height of filaments at the recovery time, t = 0 and t = 30 seconds, respectively. It can be seen that the width of filament with the recovery time, t = 0 is bigger than that at the recovery time, t = 30 seconds. This is because that most of the hydrogel's viscosity already recovered after 30 seconds of rest,

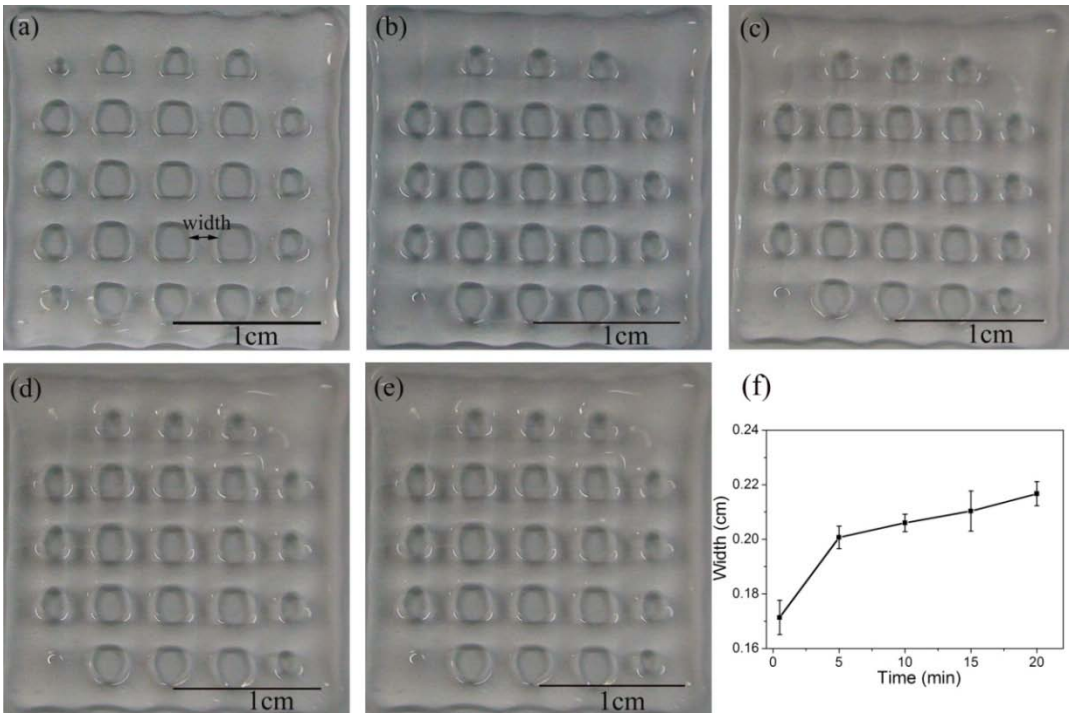

Figure 5. The images of printed hydrogel scaffolds at different ageing times. **(a)** 0.5 minutes; **(b)** 5 minutes; **(c)** 10 minutes; **(d)** 15 minutes; **(e)** 20 minutes; **(f)** the effect of ageing time on filament width for 2 wt.% alginate hydrogels added with a fixed $CaCl_2$ content of 25 mM/L.

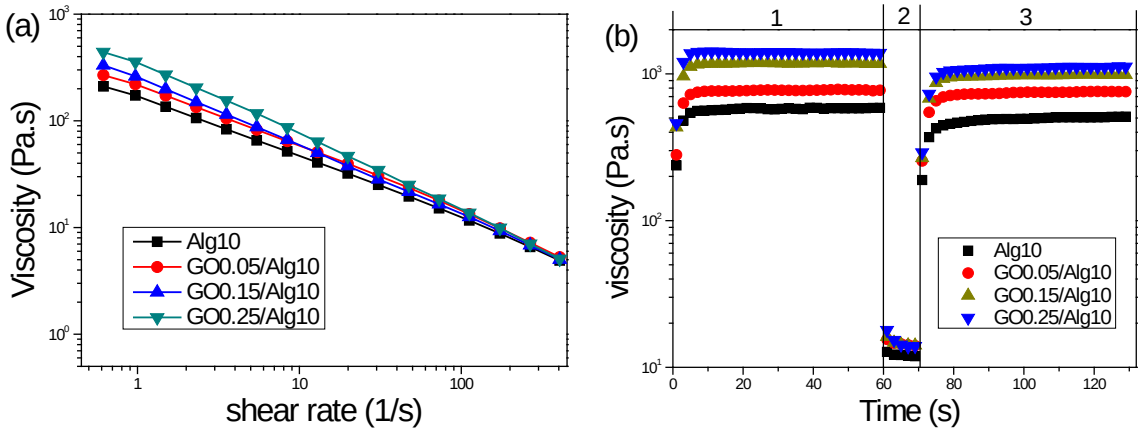

Figure 6. Effect of various GO contents on **(a)** shear-thinning behavior, and **(b)** thixotropic property of 10 wt.% alginate hydrogel.

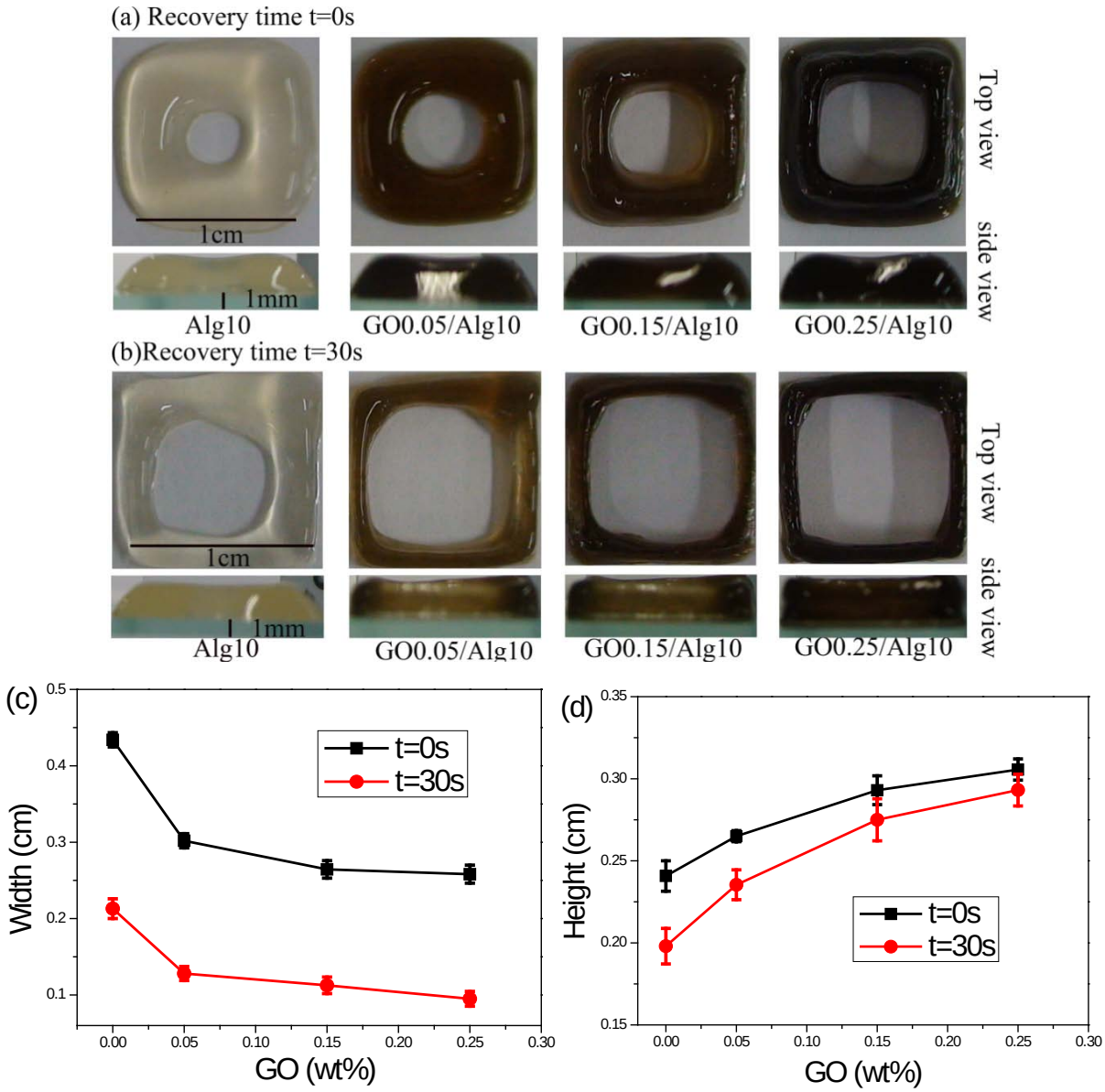

Figure 7. The morphologies of the printed scaffolds for 10 wt.% alginate hydrogels filled with various GO contents at the recovery time of **(a)** t = 0 second, and **(b)** t = 30 seconds; effect of GO content on the **(c)** width, and **(d)** height of the filament.

thus the printing quality is better for those scaffolds with a recovery time. At the same time, the filament height with a recovery time is greater than that without a recovery time. As the printed scaffold comprised of 50 layers and the printing of each layer needed to pause every 30 seconds, however, the total printing time was 1470 seconds or 24.5 minutes longer than that without taking a recovery time.

From Figure 8(a), it is observed that the value of width gradually increases with ageing time. Furthermore, as the content of GO increases from 0 to 0.25 wt.%, the time effect becomes gentle. It is because that the hydrogel with a lower concentration of GO was softer and easier to collapse and spread compared to the hydrogel with a higher GO concentration. Figure 8(b) illustrates the relationship between height and time with varying content of GO. The heights of all scaffolds decreased gradually with increment of ageing time due to the spreading effect. The height of a scaffold with more GO was always bigger than those scaffolds with lower GO contents during the observation period (20 minutes).

Figure 9 shows the effects of ageing time on the width and height of the filaments for 10 wt.% alginate hydrogels filled with various GO contents at the recovery time, t = 30 seconds. It can be found that the

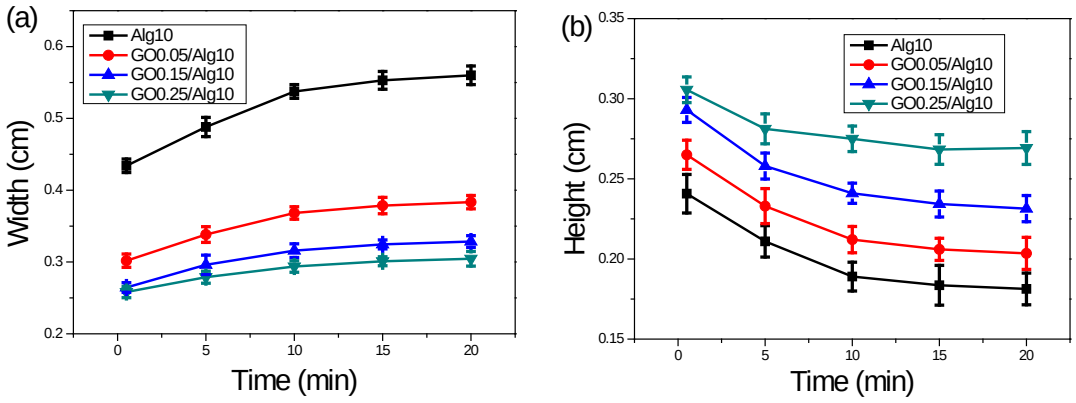

Figure 8. The relationship between **(a)** width and **(b)** height of the filaments with ageing time for alginate hydrogels filled with various GO contents at the recovery time, t = 0 second.

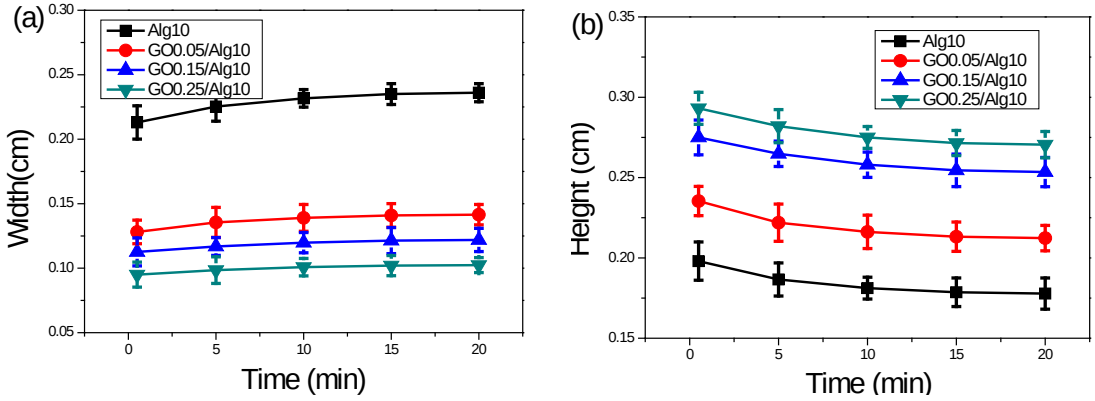

Figure 9. The relationship between **(a)** width and **(b)** height of the filament with ageing time for alginate hydrogels filled with various GO contents at the recovery time, t = 30 seconds.

width gradually increases as the ageing time increases. In comparison to the recovery time, t = 0 second (Figure 8), it is easy to find that the scaffolds printed with the recovery time, t = 30 seconds have a better quality. The recovery time also possesses an effect on the height (Figure 9(b)). The scaffolds printed with the recovery time showed gentler decreased in height with ageing time than those scaffolds printed without taking a recovery time. This is because the constructs printed with the recovery time were stronger, and thus the spread effect became less obvious than those printed without a recovery time. Therefore, printing of 3D scaffolds with hydrogels similar to GO-filled alginate hydrogels using an extrusion-based 3D printer would take a certain recovery time before printing on the other layer, and thus enable it to increase the quality of printing.

4. Conclusion

In this work, alginate-based hydrogels were prepared, and its rheological properties as well as 3D printability have been studied. We first investigated the effects of $CaCl_2$ content and alginate concentration on the gelation properties of alginate in aqueous solution. The gel point was determined using the Winter-Chambon method. It was found that the critical concentration of $CaCl_2$ at the gel point increased linearly with increasing alginate concentration, indicating that much more $CaCl_2$ are required to cross-link alginate chains into gel networks at a higher alginate concentration. The alginate/$CaCl_2$ hydrogels showed a shear-thinning characteristic, but the shear-thinning or thixotropic properties of alginate/$CaCl_2$ hydrogels were not significant enough for 3D printing. The thixotropic property and recovery time of the alginate hydrogels were known to be important to control the printability. The thixotropic property tells us how quickly and how much viscosity of a hydrogel can recover after printing, while the recovery time is the time given to the hydrogel for recovering its viscosity during a 3D printing process. While the alginate hydrogel is not an ideal biomaterial for 3D printing with an extrusion-based printer due to

its low ability of viscosity recovery, the viscosity recovery of alginate hydrogel could be improved by adding up a small amount of graphene oxide. Some measureable parameters have been defined to describe and discuss the quality of 3D printing. The present study provides a new approach to the analysis of 3D printability of a hydrogel.

Conflict of Interest and Funding

No conflict of interest was reported by the authors. This work was supported by the Academic Research Fund Tier 1 (RG100/13) from the Ministry of Education, Singapore.

References

1. Ozbolat I T and Yu Y, 2013, Bioprinting toward organ fabrication: Challenges and future trends. *IEEE Transactions on Biomedical Engineering*, vol.60(3): 691–699. http://dx.doi.org/10.1109/TBME.2013.2243912
2. Zhang Y, Tse C, Rouholamin D, *et al*., 2012, Scaffolds for tissue engineering produced by inkjet printing. *Open Engineering*, vol.2(3): 325–335. http://dx.doi.org/10.2478/s13531-012-0016-2
3. Murphy S V and Atala A, 2014, 3D bioprinting of tissues and organs. *Nature Biotechnology*, vol.32: 773–785. http://dx.doi.org/10.1038/nbt.2958
4. Billiet T, Vandenhaute M, Schelfhout J, *et al*., 2012, A review of trends and limitations in hydrogel-rapid prototyping for tissue engineering. *Biomaterials*, vol.33(26): 6020–6041. http://dx.doi.org/10.1016/j.biomaterials.2012.04.050
5. Cohen D L, Tsavaris A M, Lo W M, *et al*., 2008, Improved quality of 3D-printed tissue constructs through enhanced mixing of alginate hydrogels. *Proceedings of the Nineteenth Solid Freeform Fabrication Symposium*, 676–685.
6. Jia J, Richards D J, Pollard S, *et al*., 2014, Engineering alginate as bioink for bioprinting. *Acta Biomaterialia*, vol.10(10): 4323–4331. http://dx.doi.org/10.1016/j.actbio.2014.06.034
7. Kirchmajer D M, Gorkin III R and in het Panhuis M, 2015, An overview of the suitability of hydrogel-forming polymers for extrusion-based 3D-printing. *Journal of Materials Chemistry B*, vol.3(20): 4105–4117. http://dx.doi.org/10.1039/C5TB00393H
8. Landers R, Hübner U, Schmelzeisen R, *et al*., 2002, Rapid prototyping of scaffolds derived from thermoreversible hydrogels and tailored for applications in tissue engineering. *Biomaterials*, vol.23(23): 4437–4447. http://dx.doi.org/10.1016/S0142-9612(02)00139-4
9. Song S J, Choi J, Park Y D, *et al*., 2010, A three-dimensional bioprinting system for use with a hydrogel-based biomaterial and printing parameter characterization. *Artificial Organs*, vol.34(11): 1044–1048. http://dx.doi.org/10.1111/j.1525-1594.2010.01143.x
10. Zhu J and Marchant R E, 2011, Design properties of hydrogel tissue-engineering scaffolds. Expert Review of Medical Devices, vol.8(5): 607–626. http://dx.doi.org/10.1586/erd.11.27
11. Fan J, Shang Y, Yuan Y, *et al*., 2010, Preparation and characterization of chitosan/galactosylated hyaluronic acid scaffolds for primary hepatocytes culture. *Journal of Materials Science: Materials in Medicine*, vol.21(1): 319–327. http://dx.doi.org/10.1007/s10856-009-3833-y
12. Hunt J A, Chen R, van Veen T, *et al*., 2014, Hydrogels for tissue engineering and regenerative medicine. *Journal of Materials Chemistry B*, vol.2(33): 5319–5338. http://dx.doi.org/10.1039/C4TB00775A
13. Beyer M, Reichert J, Heurich E, *et al*., 2010, Pectin, alginate and gum arabic polymers reduce citric acid erosion effects on human enamel. *Dental Materials*, vol.26(9): 831–839. http://dx.doi.org/10.1016/j.dental.2010.04.008
14. Li Z, Ramay H R, Hauch K D, *et al*., 2005, Chitosan–alginate hybrid scaffolds for bone tissue engineering. *Biomaterials*, vol.26(18): 3919–3928. http://dx.doi.org/10.1016/j.biomaterials.2004.09.062
15. Bao H, Pan Y, Ping Y, *et al*., 2011, Chitosan-functionalized graphene oxide as a nanocarrier for drug and gene delivery. *Small*, vol.7(11): 1569–1578. http://dx.doi.org/10.1002/smll.201100191
16. Rodríguez-González C, Martínez-Hernández A L, Castaño V M, *et al*., 2012, Polysaccharide nanocomposites reinforced with graphene oxide and keratin-grafted graphene oxide. *Industrial and Engineering Chemistry Research*, vol.51(9): 3619–3629. http://dx.doi.org/10.1021/ie200742x
17. Fan H, Wang L, Zhao K, *et al*., 2010, Fabrication, mechanical properties, and biocompatibility of graphene-reinforced chitosan composites. *Biomacromolecules*, vol.11(9): 2345–2351. http://dx.doi.org/10.1021/bm100470q
18. Sui Z, Zhang X, Lei Y, *et al*., 2011, Easy and green synthesis of reduced graphite oxide-based hydrogels. *Carbon*, vol.49(13): 4314–4321. http://dx.doi.org/10.1016/j.carbon.2011.06.006
19. Chen H, Müller M B, Gilmore K J, *et al*., 2008, Mechanically strong, electrically conductive, and biocompatible graphene paper. *Advanced Materials*, vol.20(18): 3557–3561. http://dx.doi.org/10.1002/adma.200800757

20. Meyer J C, Geim A K, Katsnelson M I, *et al*., 2007, The structure of suspended graphene sheets. *Nature*, vol.446: 60–63. http://dx.doi.org/10.1038/nature05545
21. Ionita M, Pandele M A and Iovu H, 2013, Sodium alginate/graphene oxide composite films with enhanced thermal and mechanical properties. *Carbohydrate Polymers*, vol.94(1): 339–344. http://dx.doi.org/10.1016/j.carbpol.2013.01.065
22. Chung J H Y, Naficy S, Yue Z, *et al*., 2013, Bio-ink properties and printability for extrusion printing living cells. *Biomaterials Science*, vol.1(7): 763–773. http://dx.doi.org/10.1039/c3bm00012e
23. Liu Y, Ling S, Wang S, *et al*., 2014, Thixotropic silk nanofibril-based hydrogel with extracellular matrix-like structure. *Biomaterials Science*, vol.2(10): 1338–1342. http://dx.doi.org/10.1039/C4BM00214H
24. Ohsedo Y, Oono M, Saruhashi K, *et al*., 2014, A new composite thixotropic hydrogel composed of a low-molecular-weight hydrogelator and a nanosheet. *RSC Advances*, vol.4(84): 44837–44840. http://dx.doi.org/10.1039/C4RA08542F
25. Talbot E L, Yang L, Berson A, *et al*., 2014, Control of the particle distribution in inkjet printing through an evaporation-driven sol–gel transition. *ACS Applied Materials and Interfaces*, vol.6(12): 9572–9583. http://dx.doi.org/10.1021/am501966n
26. Barnes H A, 1997, Thixotropy—a review. *Journal of Non-Newtonian Fluid Mechanics*, vol.70(1–2): 1–33. http://dx.doi.org/10.1016/S0377-0257(97)00004-9
27. Chhabra R P and Richardson J F, 2011, *Non-Newtonian flow and Applied Rheology: Engineering Applications*, 2nd edn, Elsevier, UK.
28. Coulson J M, Richardson J F, Backhurst J R, *et al*., 1999, *Coulson and Richardson's Chemical Engineering Volume 1–Fluid Flow, Heat Transfer and Mass Transfer*, 6th edn, Elsevier, Oxford, UK.
29. Winter H H and Chambon F, 1986, Analysis of linear viscoelasticity of a crosslinking polymer at the gel point. *Journal of Rheology (1978–present)*, vol.30(2): 367 –382. http://dx.doi.org/10.1122/1.549853
30. Li L and Aoki Y, 1997, Rheological images of poly(vinyl chloride) gels. 1. The dependence of sol −gel transition on concentation. *Macromolecules*, vol.30(25): 7835 –7841. http://dx.doi.org/10.1021/ma971045w
31. Te Nijenhuis K and Winter H H, 1989, Mechanical properties at the gel point of a crystallizing poly(vinyl chloride) solution. *Macromolecules*, vol.22(1): 411–414. http://dx.doi.org/10.1021/ma00191a074
32. Habas J-P, Pavie E, Lapp A, *et al*., 2004, Understanding the complex rheological behavior of PEO–PPO–PEO copolymers in aqueous solution. *Journal of Rheology (1978–present)*, vol.48(1): 1–21. http://dx.doi.org/10.1122/1.1634988
33. Liu S, Yu W and Zhou C, 2013, Solvents effects in the formation and viscoelasticity of DBS organogels. *Soft Matter*, vol.9(3): 864–874. http://dx.doi.org/10.1039/C2SM27030G
34. Tadros T F, 2011, *Rheology of Dispersions: Principles and Applications*, John Wiley & Sons, New Jersey, US.